

## Synthesis and stabilization of ZnO nanoparticles on a glass plate to study the removal efficiency of acid red 18 by hybrid advanced oxidation process (ultraviolet/ZnO/ultrasonic)

Mohammad Malakootian<sup>a,b</sup>, Alireza Nasiri<sup>a</sup>, Amir Naser Alibeigi<sup>c</sup>, Hakimeh Mahdizadeh<sup>b</sup>, Majid Amiri Gharaghani<sup>c,\*</sup>

<sup>a</sup>Environmental Health Engineering Research Center, Kerman University of Medical Sciences, Kerman, Iran, Tel. +98 343 132 5128; Fax: +98 343 132 5105; emails: amiri.majid76@gmail.com (M.A. Gharaghani), m.malakootian@yahoo.com (M. Malakootian), nasiri\_a62@yahoo.com (A. Nasiri)

<sup>b</sup>Department of Environmental Health, School of Public Health, Kerman University of Medical Sciences, Kerman, Iran, email: h.mahdizadeh2018@gmail.com

<sup>c</sup>Department of Environmental Health Engineering, Sirjan School of Medical Science, Sirjan, Iran, email: amirnaser.alibeigi@gmail.com

Received 20 February 2019; Accepted 26 July 2019

### ABSTRACT

The aim of this study was to determine the amount of Acid Red 18 removal by the sonophotocatalyst process using ZnO nanoparticles. The ZnO nanoparticles were synthesized by the hydrothermal method and placed on a glass plate. The structure of the nanoparticles was investigated by XRD, TEM, BET, EDS, and SEM, and the effects of the processes involved in the sonophotocatalyst process (photolysis, adsorption, sonolysis, sonocatalysis, and photocatalysis) were compared. The highest removal rate was 94% at the initial concentration of Acid Red 18 (25 mg/L) in pH = 10 and catalyst concentration of 1.66 g/L during 45 min. The mineralization of AR 18 was confirmed by chemical oxygen demand and total organic carbon measurements. Acid Red 18 degradation by the sonophotocatalyst process followed the pseudo-first-order kinetics ( $R^2 = 0.97$ ). The stability of the synthesized and stabilized ZnO nanoparticles was investigated during five cycles (investigation reusability) in this process, and it was found that these nanoparticles have high stability. Therefore, the sonophotocatalyst process as a hybrid advanced oxidation process with high efficiency in a short period of time is able to degrade and remove resistant organic pollutants from the environment and can be employed in industrial applications.

*Keywords:* Sonophotocatalyst; Stabilization; Acid Red 18; Textile sewage; Advance oxidation process

### 1. Introduction

The textile industry produces highly colored wastewater containing organic and inorganic pollutants. The release of colored wastewater containing large amounts of organic materials into receiving waters is a major concern associated with industrial pollution. The presence of these compounds in industrial wastewater, especially textile wastewater,

requires searching for a suitable process to reduce the number of pollutants to a standard level in surface and underground waters.

Azo dyes are among the synthetic dyes used in many textile industries [1–3], widely used due to the presence of the (–N=N–) group in their structure as well as their low cost, high solubility, and high stability [2]. Azo dyes and the intermediate products resulting from their degradation are toxic, carcinogenic, and mutagenic for marine life. Therefore, the removal of dye from textile industry wastewater is an

\* Corresponding author.

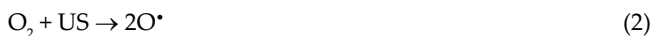
This article was originally published with an error in an author's affiliation. This version has been corrected. Please see Corrigendum in vol. 172 (2019) 429 [10.5004/dwt.2019.25359].

important step in controlling environmental pollution. Due to the high resistance of dyes to biological degradation, their slow rate of degradation, the presence of aromatic rings, and the toxicity of many dyes for microorganisms, it is essential to use physicochemical processes to remove these compounds [4,5]. Several methods such as adsorption, absorption, chlorination, ozonation, electrochemical, biodegradation, and advanced oxidation processes (AOPs) have been proposed for the treatment of colored wastewater from textile industries [6]. Therefore, the use of processes for the removal of pollutants or their oxidation to harmless by-products is a priority.

AOPs have been developed for the degradation of organic pollutants. In general, AOPs are oxidation and degradation reactions in which free radicals, such as hydroxyl, break down organic materials and convert them into simpler mineral compounds such as carbon dioxide (CO<sub>2</sub>) and water [7–11].

Recently, the ultrasonic process has been applied as a green technology to remove water and wastewater pollutants. This process reduces the pollutant load through acoustic cavitations and consequently chemical and physical changes in the solution [8].

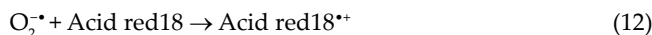
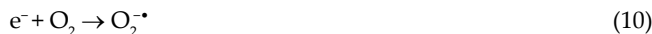
The ultrasonic cavitation process has been presented as a substitute for other pollutant treatment processes due to the degradation of pollutants without secondary contamination. When using ultrasonic techniques, the sonolysis of water molecules and, in case of presence of an oxygen molecule, thermal degradation, produces different reactive species such as OH<sup>•</sup>, H<sup>•</sup>, and hydro-peroxide (OOH<sup>•</sup>) radicals with a high degradation power. The corresponding reactions are presented in Eqs. (1)–(5) [9,10,12–14].



Several studies have demonstrated the potential of the ultrasonic technique for pollutant degradation in wastewater [13,15–19]. However, it has been revealed that the rate of pollutant degradation and removal is relatively slow when using the ultrasonic process alone [20]. As a result, efforts have been made to increase degradation efficiency using hybrid techniques. Hybrid processes are utilized to combine the ultrasonic technique with other AOPs such as photocatalyst to increase the degradation efficiency of pollutants [8,9,20,21].

AOPs using heterogeneous catalysts as photocatalysts are applied to degrade harmful, hazardous, resistant, and toxic materials produced in daily life and in the environment. In photocatalytic processes, semiconductors such as titanium dioxide (TiO<sub>2</sub>) or zinc oxide (ZnO) are exposed to ultraviolet radiation, leading to the production of active hydroxyl radicals for the removal of organic pollutants [10,22,23].

ZnO is used more than other semiconductor photocatalysts due to its high photosensitivity, proper stability, non-toxicity for marine life, high efficiency in electron production, and high ability to absorb a wide range of electromagnetic waves [24]. ZnO, which is involved in the oxidation and reduction process, is stimulated by the energy from violet light or the Sun. By irradiating on the catalyst surface, the UV light energy excites the valence electrons and enables electron transfer from the valence band (V<sub>B</sub>) to the conduction band (C<sub>B</sub>). This electron transfer leads to the formation of an electron–hole pair. The electron–hole pairs react with a hydroxide ion (OH<sup>-</sup>) or a water molecule to form hydroxyl radicals (OH<sup>•</sup>) [7,22,25].



Catalysts in the photocatalytic process are employed in suspension and stabilized forms [23]. The stabilization of ZnO nanoparticles on an inorganic medium can both increase the catalyst life in the reactor and enhance the potential for catalyst reuse. Two basic problems, including difficult recycling and UV light dispersion that occur when nanoparticles are used as a suspension in the photocatalytic process, are resolved by the stabilization of nanoparticles on a plate such as glass [26,27].

The combination of photocatalyst and ultrasonic techniques, known as the sonophotocatalyst hybrid process [8], will provide more free radicals for the reaction, resulting in increased degradation [10,21]. The synergistic effect of ultrasound and UV irradiation plus stabilized nanoparticles increases free radical formation in the aqueous solution, enhances the formation of bubble cavities, accelerates and facilitates the mass transfer of pollutant molecules onto the photocatalyst surface and, as a result, promotes the removal of impurities [21]. Therefore, the aim of this study was to synthesize ZnO nanoparticles and stabilize them on glass as the medium, and then apply photocatalyst and ultrasonic techniques for the removal of Acid Red 18 from aqueous solutions through the hybrid oxidation process.

## 2. Experimental procedure

### 2.1. Materials

Zinc sulfate (ZnSO<sub>4</sub>·7H<sub>2</sub>O, 99.5%), sodium carbonate (Na<sub>2</sub>CO<sub>3</sub>, 99.9%), double distilled water, ethanol (CH<sub>3</sub>CH<sub>2</sub>OH,

99.5%), sodium hydroxide (NaOH), and sulfuric acid (H<sub>2</sub>SO<sub>4</sub>) with a high purity percentage were purchased from Merck Company (Germany). Moreover, Acid Red 18 (>99% purity) was purchased from Alvan Sabet Co. (Hamadan, Iran). The characteristics of the dye are presented in Table 1.

## 2.2. Synthesis of ZnO nanoparticles

ZnO nanoparticles were synthesized using the thermal method. We prepared the 0.5 M zinc sulfate (ZnSO<sub>4</sub>·7H<sub>2</sub>O) solution in double distilled water. Then, 0.4 M sodium carbonate solution was added to the zinc sulfate solution dropwise with vigorous stirring at 70°C for 45 min to form Zn<sub>4</sub>(SO<sub>4</sub>)(OH)<sub>6</sub>·0.5 H<sub>2</sub>O. The white precipitate was collected by filtering and then washed several times with distilled water and ethanol. It was then placed in an oven at 70°C to dry. Finally, the precursors were calcinated at 825°C for 1 h [28] (Fig. 1).

## 2.3. Nanoparticle stabilization on a glass plate

Three glass plates with the dimensions of 3 × 20 cm were used as the surface for the stabilization of ZnO nanoparticles. The surface of the glasses was employed as a medium for the better bonding of ZnO nanoparticles to the sandblast. Afterwards, for activating the glass surface and for better stabilization, the glasses were placed in concentrated sodium hydroxide for 24 h. After removing the glass plates from the concentrated sodium hydroxide solution, they were washed several times with deionized water until the pH of the water reached 7. The plates were dried at room temperature. Next, the synthesized nanoparticles were uniformly coated on the glass surface. It was then dried at room temperature for 24 h. Finally, for the calcination of the coated glass plates, they were placed in an electric furnace at 850°C (BADi) for 1 h, and were then removed from the furnace and stored in aluminum foils for the following steps of the test [27–29].

## 2.4. Description of the reactor

To conduct the test, we used a 500-mL reactor made of Plexiglas with three UV-C lamps installed above it (Fig. 2). The reactor was placed inside an ultrasonic device. Glass plates containing stabilized ZnO were placed inside the reactor. Eventually, the contents of the reactor were mixed with a peristaltic pump.

## 2.5. Photocatalytic study

A synthetic sample (1,000 mg/L of Acid Red 18 powder in 1 L of distilled water) was prepared. First, the effects of the processes involved in the sonophotocatalyst process (i.e., photolysis, adsorption, photocatalysis, photolysis + sonolysis, and sonophotocatalysis) were investigated at 25 mg/L concentration of Acid Red 18 with a pH of 7 for 45 min. After that, the effects of pH (3, 7, and 10), Acid Red 18 concentration (25, 50, 75, and 100 mg/L), catalyst concentration (1, 1.66, 2.33, and 3 g/L) and reaction time (5, 10, 15, 20, 25, 30, 35, 40, and 45 min) were evaluated on the sonophotocatalyst hybrid process and the removal efficiency of Acid Red 18. Afterwards, the optimal conditions for dye removal were determined. The duration of the test was 45 min, and the sampling was performed in 5, 10, 15, 20, 25, 30, 35, 40, and 45 min intervals. For pH adjustment, sulfuric acid and sodium hydroxide were used in all the experiments.

The concentration of the Acid Red 18 residue in the solution was measured by a UV/Vis spectrophotometer at the maximum wavelength of 507 nm. The degradation and dye removal ( $\eta$ ) rates were calculated using the equation below.

$$\eta = \frac{C_0 - C_t}{C_0} \times 100 \quad (14)$$

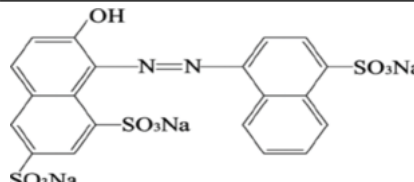
where  $C_0$  is the initial concentration and  $C_t$  is the concentration of the dye at each moment of the sampling.

To determine the adsorption rate of the synthesized nanoparticles before the outset of the process, the prepared solution was placed in a dark environment for 30 min in contact with stabilized nanoparticles until the surface of the nanoparticles was saturated with dye molecules and reached equilibrium. The kinetics of the sonophotocatalyst hybrid reaction of aqueous organic compounds such as dye can be expressed by the Langmuir–Hinshelwood model. This model is essentially related to degradation rate and dye concentration, as expressed in Eq. (15).

$$r = \frac{dc}{dt} \times \frac{K_r K_{ad} C}{1 + K_{ad} C} \quad (15)$$

Here,  $K_{ad}$  denotes the absorption equilibrium constant,  $K_r$  indicates reaction rate constants, and  $C$  is the organic matter concentration. When the concentration of the compounds is low, Eq. (16) can be simplified to express the pseudo-first-order kinetics with a known rate constant ( $K$ ) [12].

Table 1  
Properties of the Acid Red 18 dye

Molecular mass (g/mol)	Type of dye	Maximum wavelength (nm)	Chemical formula	Chemical structure
604.47	Mono-Azo	507	C <sub>20</sub> H <sub>11</sub> N <sub>2</sub> Na <sub>3</sub> O <sub>10</sub> S <sub>3</sub>	

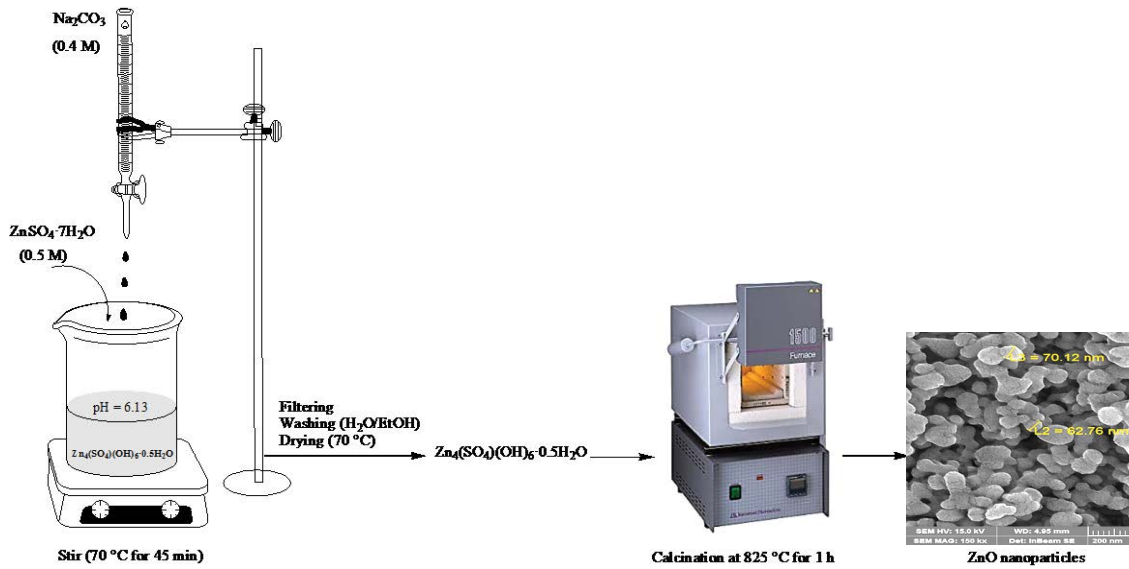


Fig. 1. Experimental procedure for the synthesis of nano-ZnO.

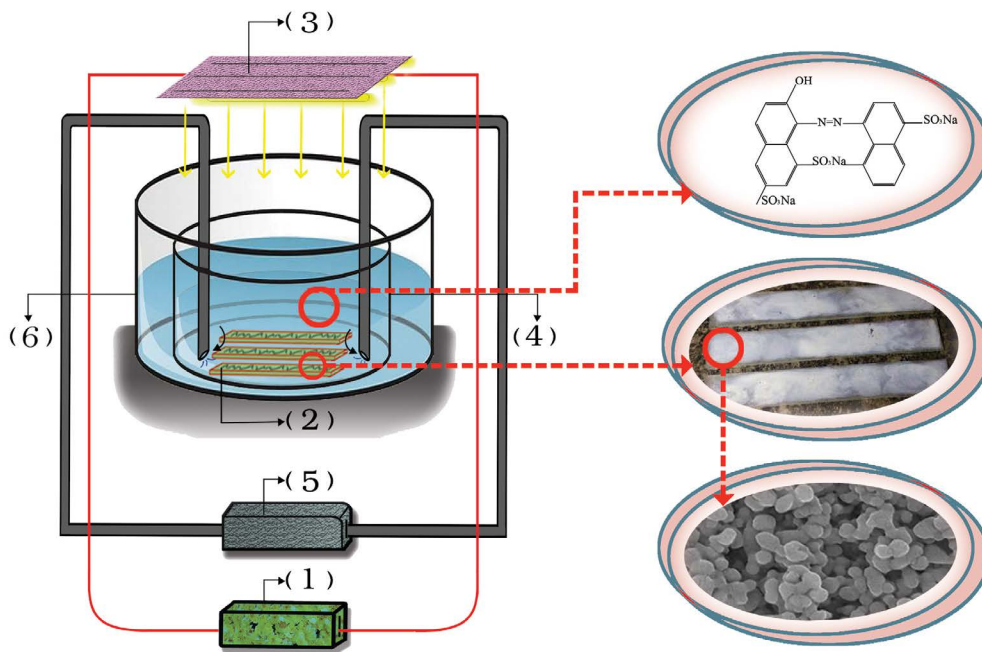


Fig. 2. The system used for performing the sonophotocatalytic process (1. Transformer, 2. ZnO nanoparticles stabilized on the surface of glass, 3. UV-C lamp, 4. Plexiglass, 5. Peristaltic pump, 6. Ultrasonic device).

$$\ln\left(\frac{C}{C_0}\right) = Kt \tag{16}$$

If the  $\ln(C/C_0)$  graph vs. reaction time is a straight line, the graph slope indicates the rate constant ( $K$ ).

The decomposition rate of acid red 18 was determined on the basis of changes in the UV/Vis spectra (Shimadzu, Japan), the removal efficiency of chemical oxygen demands (COD), and the removal efficiency of total organic carbon

(TOC) (TOC analyzer, Jena-C3100, Germany). The COD tests were conducted using recycled distillation based on the C5220 method (the 20th edition of the Standard Methods for the Examination of Water and Wastewater). The COD test was performed to determine the mineralization of colored organic matter by titration. COD was measured using Eq. (17). The sample harvested with  $HgSO_4$  was titrated in the presence of  $K_2Cr_2O_7$ ,  $Ag_2SO_4$ , and  $H_2SO_4$  and refluxed for 2 h with ferric ammonium sulfate. Also, the Ferroin indicator was utilized as a reflux. The titration

of the blank sample was performed using distilled water instead of a dye sample [24].

$$\text{COD} = \frac{(\text{Blank titre value} - \text{dye sample titre value}) \times \text{normality of FAS} \times 8 \times 1000}{\text{Volume of sample}} \quad (17)$$

Recycling and re-use of the stabilized catalyst were also investigated. Each time, the nanoparticles stabilized on the glass plate were washed with distilled water and ethanol and used with a sonophotocatalyst process to degrade Acid Red 18. All the tests were performed in triplicate, and the average was reported.

### 2.6. Analysis

The microstructures, morphologies, and chemical compositions of nano-ZnO were investigated by a scanning electron microscope (Vega, TESCAN, USA) and energy dispersive spectroscopy (EDS) (MIRA3 TESCAN-XMU). Using X-ray diffraction (XRD) patterns, the purity of synthesized ZnO was studied by an XRD anode Cu system ( $\lambda$ : 1.54056 Å) within the range of  $2\theta$  from  $10^\circ$  to  $80^\circ$  and with the step size of 0.026 S (GNR, MP 3000, Italy). The solution pH was measured using a digital pH meter (Hanna Instruments, Japan). An ultrasonic device (Elmasonic S 60 H, Germany) was employed to produce sound waves. Three UV-C lamps were also used to produce ultraviolet radiation (Philips, the Netherlands). The BET surface areas were evaluated based on  $N_2$  adsorption–desorption isotherms using a specific surface analyzer (BELSORP-mini II) at  $120^\circ\text{C}$ . Finally, a transmission electron microscope (TEM: Philips CM30, the Netherlands) was applied to characterize particle size and morphology.

## 3. Results and discussion

### 3.1. Structural and surface properties of ZnO nanoparticles

#### 3.1.1. XRD

The crystal structure of ZnO nanoparticles stabilized on a glass plate was used for XRD analysis and the results are exhibited in Fig. 3. Evidently, all peaks are

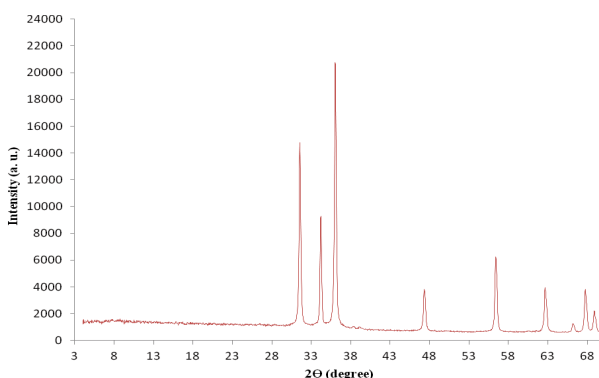


Fig. 3. XRD pattern of thermally-synthesized nanoparticles stabilized on a glass plate.

consistent with the XRD patterns of nanoparticles noted by other researchers [24,30]. The lack of extra peaks in the XRD spectrum indicates the high purity percentage of the synthesized and stabilized nanoparticles. Peaks at 100-002-101-102-110-103-200-112-201-004-202 reveal that the structure of ZnO is hexagonal, which is according to standard ranges of (JCPDS card no. 36-1451: Joint Committee Powder Diffraction Standards). Furthermore, the presence of high-intensity and narrow peaks indicates the crystal properties of ZnO nanoparticles [29]. Previously, Srivastava et al. [31] synthesized nano-ZnO in an aqueous medium and estimated the structure of nanoparticles with XRD, which is similar to the present study.

These XRD patterns indicated the presence of a hexagonal wurtzite structure of ZnO nanoparticles. The average crystalline size of ZnO nanoparticles was calculated using the Debye–Scherrer’s equation (Eq. (18)).

$$D = \frac{0.9\lambda}{\beta \cos\theta} \quad (18)$$

where  $\beta$  is the line broadening at the full width at half maximum (FWHM) of the most intense peak,  $\theta$  is the Bragg angle, and  $\lambda$  is the X-ray wavelength. The crystalline size of ZnO nanoparticles calculated using the Debye–Scherrer’s equation was found to be 6–7 nm.

#### 3.1.2. SEM

Fig. 4 displays the SEM image of ZnO nanoparticles synthesized and stabilized on a glass plate. The particles are almost spherical in shape and there is a uniform coating of the nanoparticles on the glass plate. SEM images of ZnO samples show that the density of particles is normal in the thermal synthesis and stabilization method.

#### 3.1.3. Energy dispersive spectroscopy analysis of synthesized ZnO nanoparticles

To check the chemical composition and purity of the synthesized ZnO nanoparticles, energy dispersive spectroscopy analysis was performed. The results revealed 82.34% Zn and 17.66% O in accordance with the expected values for confirming the chemical structure of nano-ZnO (Fig. 5).

#### 3.1.4. TEM

To determine the actual size and morphology of the particles, samples were systematically analyzed by TEM. Fig. 6 illustrates the TEM image of ZnO nanoparticles immobilized on a glass plate. The image also presents the small size of ZnO nanoparticles, which gives it a high specific surface area. Also, the TEM image confirms that the morphology of the nanoparticles is spheroid.

#### 3.1.5. Surface area and porosity analysis of the synthesized ZnO nanoparticles

The adsorption/desorption isotherm and the BET–BJH specific surface area of the synthesized ZnO nanoparticles are presented in Fig. 7. The specific surface area of the ZnO nanoparticles was  $25.504 \text{ m}^2/\text{g}$ , and the mean pore diameter and total pore volume were 12.21 nm and  $0.078 \text{ cm}^3/\text{g}$ ,

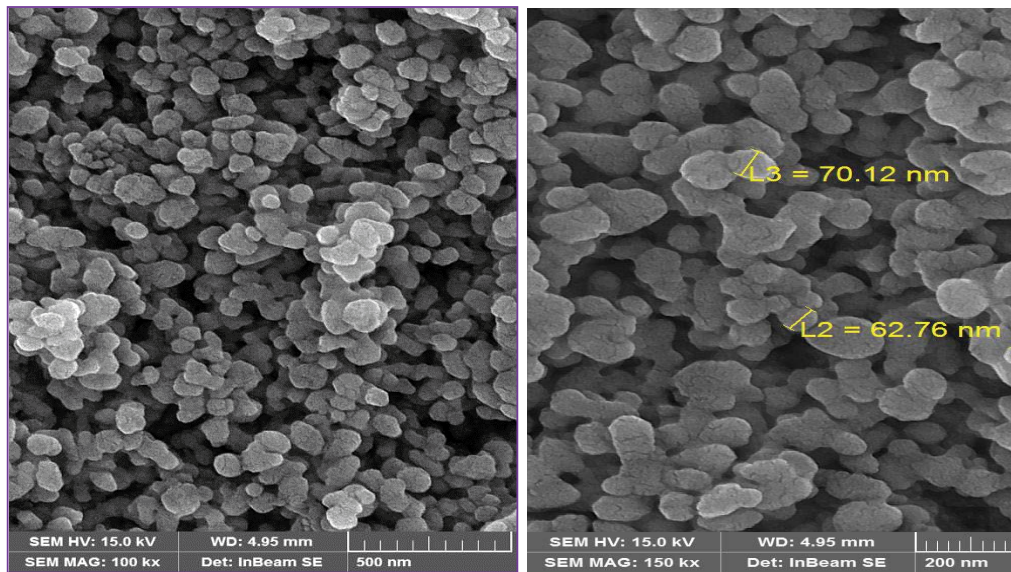


Fig. 4. SEM images of ZnO nanoparticles stabilized on a glass plate.

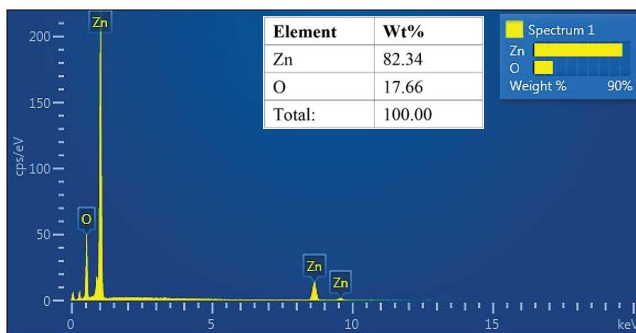


Fig. 5. EDS pattern of the synthesized ZnO nanoparticles.

respectively. Previously, Suntako [32] synthesized nano ZnO by the precipitation method in an aqueous medium, and the specific surface area of the nano-ZnO was reported to be 20.28 m<sup>2</sup>/g.

### 3.2. Influence of the parameters involved in sonophotocatalyst

Fig. 8 presents the results of the destruction and degradation of Acid Red 18 by photolysis, sonolysis, sonophotocatalysis, photocatalysis, and sonocatalysis. It can be seen that both the photocatalysis and sonophotocatalysis have the potential to degrade Acid Red 18, and the effect of sonophotocatalysis is better than that of photocatalysis and sonolysis.

By comparing the data obtained from rate constants between sonophotocatalyst as a combined process and sonocatalysis and photocatalysis as individual processes, it can be clearly observed that there is a synergistic effect in sonophotocatalysis. This effect can be revealed by the difference between rate constants in sonophotocatalysis as a combined process and the other two as separate ones, according to Eq. (19). Data are shown in Table 2.

The combined effect of sonolysis and photocatalysis with the degradation rate constant ( $k_{US+UV+ZnO}$ ) is greater than the

sum of the degradation rate constants calculated for sonolysis ( $k_{US}$ ), photocatalysis ( $k_{UV+ZnO}$ ) and sonocatalysis ( $k_{US+ZnO}$ ). In the synergistic photocatalyst and ultrasonic process, the increased amount of active surface available for catalysis enhances the production of hydroxyl radical and degradation rate [8].

$$\text{Synergy} = \frac{(k_{US+UV+ZnO}) - (k_{UV+ZnO} + k_{US+ZnO})}{k_{US+ZnO+UV}} \quad (19)$$

Photolysis and ultrasonic processes had a low degradation power. In fact, due to the low hydroxyl radical production, the degradation rate and removal efficiency were reduced [9]. In degradation through the photocatalysis process, UV irradiation on the catalyst surface excites the valence band and produces electron-hole pairs, which produces hydroxyl radicals and causes further pollutant degradation in reaction with water and hydroxide ions [22].

The main mechanisms of degradation and destruction through azo dye sonophotocatalysis are most likely due to the additional free radicals formed by H<sub>2</sub>O degradation in a cavitation bubble. These mechanisms are capable of degrading the pollutants. On the other hand, the hydrogen peroxide produced by both sonolysis (Eq. (20)) and photocatalysis in water (Eq. (21)) caused different reactions (Eqs. (22)–(25)). In this process, they produced strong hydroxyl radicals (OH<sup>•</sup>) with a high degradation power [8,13,21,33,34].



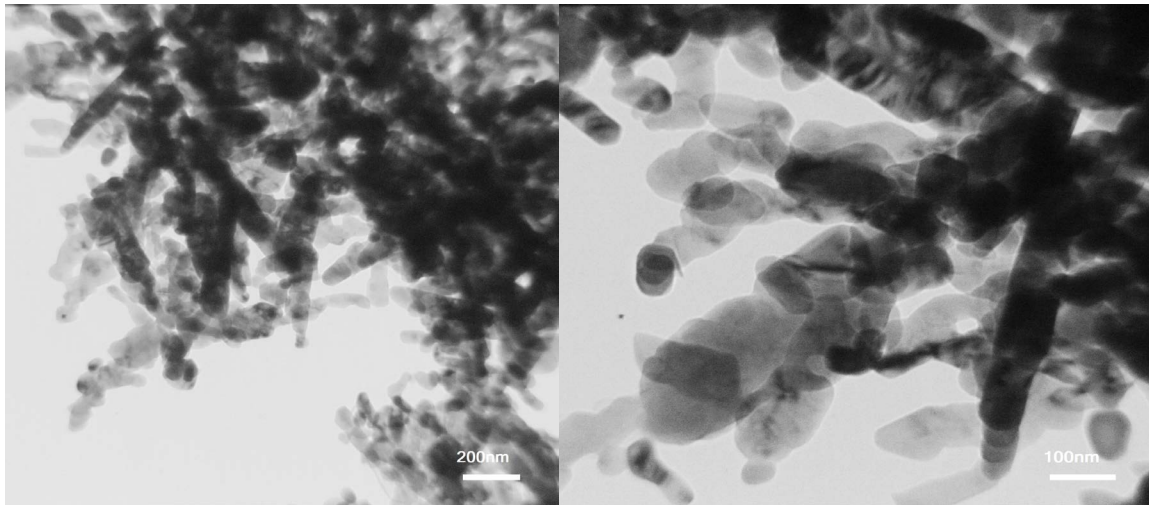


Fig. 6. TEM images of ZnO nanoparticles.

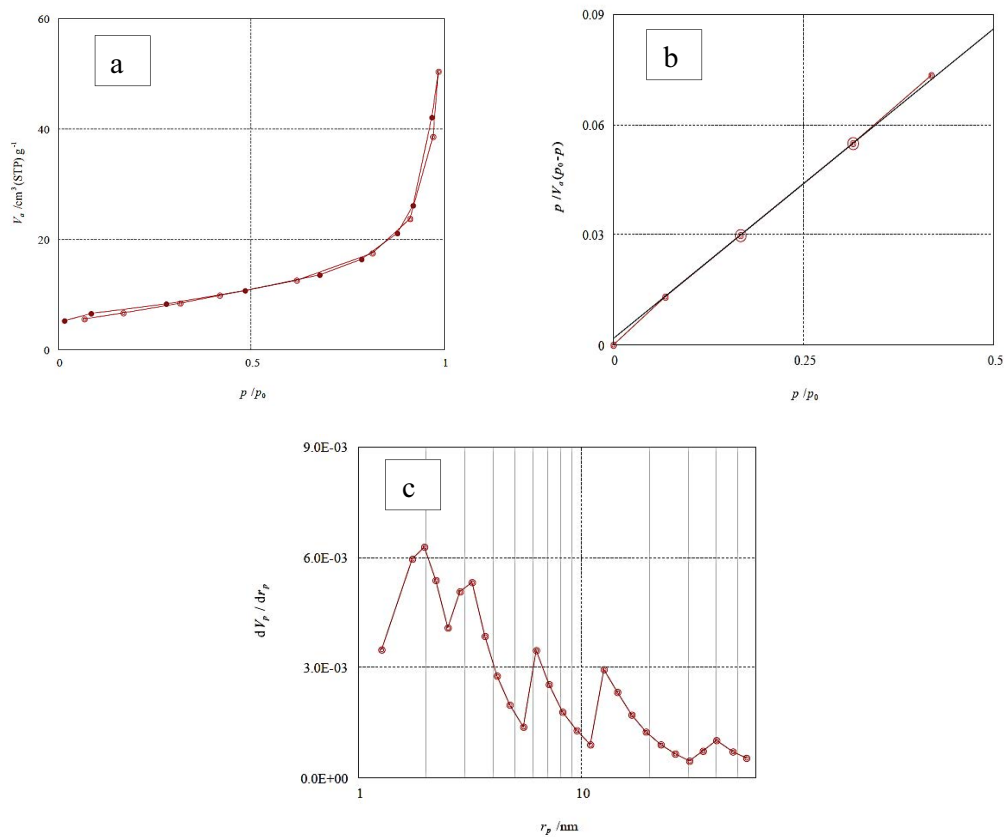
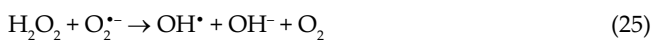


Fig. 7. (a) Adsorption/desorption isotherm, (b) BET surface area, and (c) BJH surface area of the synthesized ZnO nanoparticles.



Also, the use of the ultrasonic process increases the turbulence in the fluid which reduces mass transfer limitations, availability of catalyst surface, production of free radicals and, consequently, degradation and destruction of

pollutants. On the other hand, the catalytic activity of ZnO nanoparticles in combination with the ultrasonic process is increased, and the surface available to nanoparticles is enhanced. Another reason for the enhanced activity of photocatalytic processes in the presence of the ultrasonic process is the increased transfer of organic mass from liquid onto the

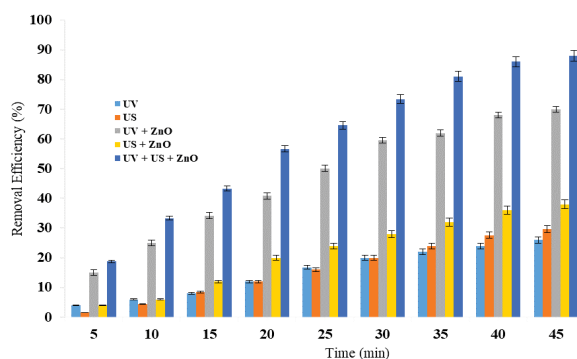


Fig. 8. Effect of various processes involved in the sonophotocatalytic degradation of Acid Red 18 at different times (initial concentration of Acid Red 18: 25 mg/L and ZnO catalyst concentration: 1.66 g/L, pH = 7).

Table 2

Pseudo-first-order rate constant in the degradation of Acid Red 18 by sonophotocatalysis, photocatalysis, and sonocatalysis

$C_0$ (mg/L)	25
$k_{UV+ZnO}$	0.0275
$k_{US+ZnO}$	0.0114
$k_{US+UV+ZnO}$	0.0487
Synergy	0.2012

catalyst surface [34,35]. Mishra and Gogate [36] compared the sonophotocatalyst hybrid and sonolysis processes in terms of pollutant removal, showing that the degradation rate significantly increases in the sonophotocatalytic process. The removal efficiency of the sonocatalytic process was more than that of sonolysis. The use of a catalyst in the presence of ultrasonic irradiation and the absence of UV irradiation is known as sonocatalysis. The temperature of “hotspot” was also created by acoustic cavitation in an aquatic medium, so that high temperature would make many holes on the surface of ZnO nanoparticles generation  $OH^\bullet$  radicals. Also, some oxygen atoms are produced on the surface of ZnO nanoparticles by the shock waves of ultrasound, leading to evaporation from the crystal lattice and then the formation of holes. As a result, these holes can directly degrade the adsorbed organic pollutant on the surface of ZnO nanoparticles or indirectly decompose them in the aqueous solution when the  $OH^\bullet$  radicals are being developed from the reaction of  $H_2O$  molecules and holes [34]. The study by Talebian et al. [21] focused on azo dye waste removal by the photocatalyst process in the compound of ultrasound. They reported that the level of azo dye removal is low in the presence of ultrasound waves in 100 min, which is less than the rate of the compound process with ZnO nanoparticles [21].

### 3.3. pH effect

Solution pH plays an important role in the photocatalytic degradation of organic pollutants in aqueous solutions since

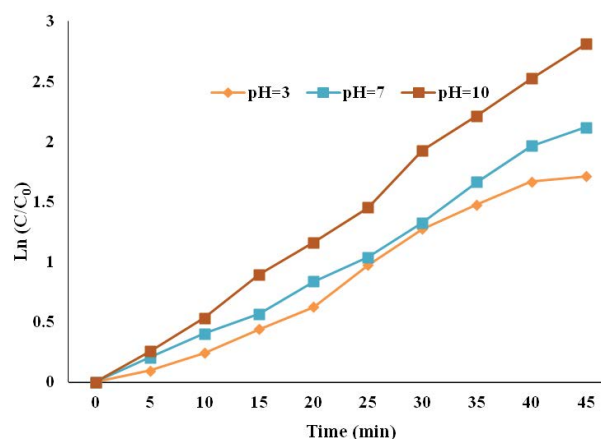


Fig. 9. Effect of pH on the removal of Acid Red 18 by the sonophotocatalyst hybrid process at different times (initial concentration of Acid Red 18 was 25 mg/L; concentration of the catalyst stabilized on a glass plate was 1.66 g/L).

it determines the surface charge of the photocatalyst and the size of the constituent ions [1]. Therefore, solution pH can play a key role in the adsorption oxidation and photocatalysis of contaminants. The effect of the pH parameter in the removal of Acid Red 18 by the sonophotocatalyst hybrid process in pH = 3, 7, and 10 is shown in Fig. 9. The pseudo-first-order rate constants in pH = 3, 7, and 10 were 0.2151, 0.2435, and 0.3212  $\text{min}^{-1}$ , respectively. Therefore, pH = 10 was chosen as the optimal value. At a high pH, the alkalinity factor is mostly due to  $OH^-$  ion, the excess of which leads to hydroxyl radical formation and increased degradation rate [37,38].

The low removal rate in acidic conditions can be attributed to the reaction of ZnO with acids and the formation of insoluble salts. Furthermore, the low degradation in acidic conditions can be attributed to the loss of OH ions by the proton, preventing the formation of hydroxyl radical. The zero point charge ( $pH_{ZPC}$ ) of the ZnO nanoparticle is 9. The particle surface at pH values > 9 has a negative charge due to the adsorption of hydroxide ions. The presence of high amounts of  $OH^-$  ions on the nanoparticle surface and the presence of these ions at the reaction time leads to the formation of hydroxyl radicals. Thus, the production of hydroxyl radicals increases Acid Red 18 degradation [1].

At neutral and alkaline pH levels, the released electrons (Eq. (6)) have the ability to react with the oxygen atom (as an electron receptor), which converts the oxygen atom from the  $O_2$  form to the  $O_2^{\bullet-}$  form (Eq. (10)). The created radicals ( $O_2^{\bullet-}$ ) attack Acid Red 18 molecules and isolate an electron and convert it to the  $AR18^+$  form (Eq. (12)) or react with the  $OH^-$  or  $H_2O$  molecule and produce a hydroxyl free radical, thereby degrading the dye [39].

### 3.4. Effect of various ZnO nanoparticle concentrations stabilized on the glass plate

The concentration of catalyst in photocatalysis processes and the sonophotocatalyst hybrid process is an important factor affecting the removal of organic pollutants. In order to prevent the excessive use of nanoparticles from an economic



point of view, it is necessary to determine the optimal concentration. The effect of the concentration of ZnO stabilized on the glass plate at the concentrations of 1, 1.66, 2.3, and 3 g/L on Acid Red 18 was shown by the sonophotocatalyst hybrid process in Fig. 10. The results demonstrated that, with increasing the nanoparticles, the removal rate is increased.

In fact, at the concentration of 2.33 g/L, the pseudo-first-order constant was  $0.083 \text{ min}^{-1}$ , while the rate constants of 1.66 and 1 g/L concentrations were  $0.0642$  and  $0.0487 \text{ min}^{-1}$ , respectively. In explaining the reason for the enhanced removal efficiency of Acid Red 18 by increasing the concentration of nanoparticles, it can be stated that, by increasing nanoparticles, active surface spots are further stimulated by UV irradiation and more hydroxyl radical is released [40]. In addition, the high concentrations of ZnO catalyst make a large amount of dye to adsorb onto the catalyst surface. On the other hand, the increased density of catalyst particles in the region under UV radiation produces hydroxyl radical and other reactive species, thereby improving dye degradation and removal [24].

According to the results, it is observed that, with increasing nanoparticle content to more than 2.33 g/L, the degradation rate and reaction rate constant decline and the rate constant at the 3 g/L concentration of ZnO nanoparticle is equal to  $0.0733 \text{ min}^{-1}$ , which indicates a steady reduction in rate with increasing nanoparticle concentration to more than 2.33 g/L. This reduction in the rate constant with the increase in the concentration of nanoparticles could be attributed to the agglomeration of concentration on the surface and, subsequently, the reduction of the number of active surface sites available for radical production [3,40]. Since the removal rate does not change with increasing ZnO nanoparticle concentration from 1.66 to 2.33 g/L, the concentration of 1.66 g/L was chosen as optimal.

### 3.5. Effect of the initial concentration of Acid Red 18

The effect of the initial concentration of the pollutant is an effective parameter in AOPs, such as photocatalysis and sonophotocatalysis. Based on Fig. 11, the efficiency of Acid Red 18 degradation sonophotocatalyst hybrid process was

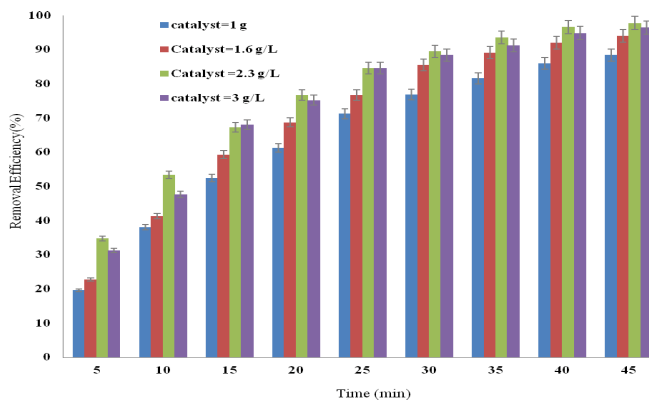


Fig. 10. Effect of ZnO nanoparticle catalyst concentration in the sonophotocatalyst hybrid process on the removal of Acid Red 18 at different times (initial concentration of Acid Red 18: 25 mg/L, pH: 10).

optimal at the concentrations of 25, 50, 75, and 100 mg/L in pH 10 and a catalyst dose of 1.66 g/L. The results indicate that the removal efficiency is reduced by increasing the concentration of Acid Red 18, such that the highest removal rate occurred at the concentration of 25 mg/L with the degradation and removal rate of 94%. The removal rates of Acid Red 18 at the 50, 75, and 100 mg/L concentrations were 82%, 75.33%, and 57.7%, respectively, by sonophotocatalyst hybrid during 45 min. The reason for the declined degradation with the increase in the concentration of Acid Red 18 may be that the reduced wavelength of the photons deposited in the solution prevents catalyst surface stimulation to produce active radicals for degradation. Moreover, by increasing Acid Red 18 concentration, more molecules are adsorbed and saturated on the surface of the catalyst, and the activity of the active sites of the catalyst surface is reduced to produce hydroxyl radicals [8,21,41]. Reduction in reaction rate with increasing the substrate concentration is attributed to an increase in adsorbed dye molecules on the catalyst surface which causes a reduction in UV light adsorption and excitation and radical production. These phenomena lead to a decrease in the cavitation of the catalyst surface by the ultrasonic process. At high concentrations, due to the saturation of the catalyst surface and production of intermediates, there is a competition between dye molecules and intermediates for occupying catalyst surface which causes a decrease in reaction rate in synergistic processes [8,42].

### 3.6. Impact of contact time

The effect of contact time on the degradation and removal of Acid Red 18 is depicted in Fig. 12. By increasing the contact time from 5 to 45 min, the degradation rate reaches from 22.75% to 94%. At times longer than 45 min, the degradation rate is slower than the previous condition. The trend of increase in removal efficiency decreased in this state. Also, according to this figure, with increasing the contact time, the amount of absorption decreases, and the peak broadens. In fact, by increasing contact time, the amount of produced

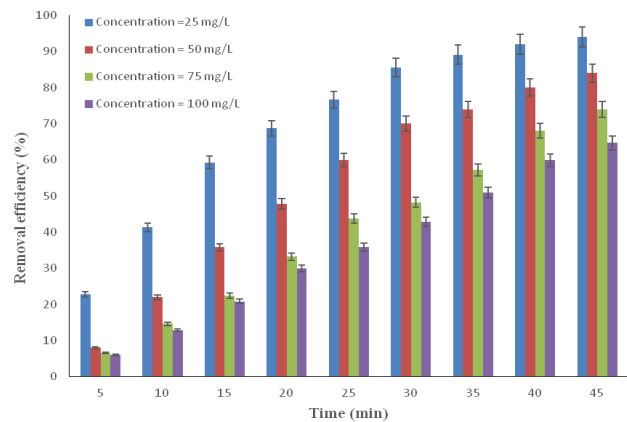


Fig. 11. Effect of the initial concentration of Acid Red 18 on the removal rate by the sonophotocatalyst hybrid process at different times (pH = 10, concentration of ZnO catalyst stabilized on the glass plate was 1.66 g/L).

hydroxyl radicals increases and, consequently, the degradation and removal rates increase [37,43].

The low degradation and removal at the above times can be attributed to the increased contact time, the increased amount of intermediate organic compounds resulting from Acid Red 18 degradation, and the use of some hydroxyl radicals for the degradation of these materials, resulting in a reduction in removal rate. The results indicate that there is no significant change in the spectral shape during the sonophotocatalyst process. The peak intensity at 507 nm wavelength during the degradation process is gradually reduced, showing that the intermediate materials do not interfere at the absorbance length of 507 nm. Table 3 presents the sonophotocatalyst degradation reaction constant for different concentrations of Acid Red 18. The sonophotocatalyst degradation process rate constants of Acid Red 18 at the concentrations of 25, 50, 75, and 100 mg/L were, respectively, 0.0642, 0.042, 0.029, and 0.023 min<sup>-1</sup>, showing that rate constant decreases as the concentration of Acid Red 18 is increased.

### 3.7. Reaction kinetics

In general, the Langmuir–Hinshelwood model was the most suitable model for describing the sonophotocatalyst process. According to the Langmuir–Hinshelwood equation, the ln(C/C<sub>0</sub>) graph was plotted against the reaction time. With respect to Fig. 13, for each concentration of Acid Red

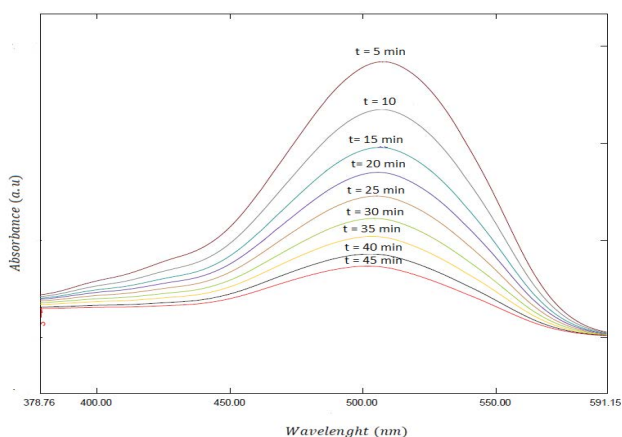


Fig. 12. UV-Vis absorption spectra changes of the Acid Red 18 by the sonophotocatalyst hybrid process at different times (initial concentration of Acid Red 18 was 25 mg/L, pH = 10, concentration of ZnO catalyst stabilized on the glass plate was 1.66 g/L).

Table 3

Results of the kinetics of pseudo-first-order reaction by the sonophotocatalyst hybrid process at various concentrations of Acid Red 18

C <sub>0</sub> (mg/L)	R <sup>2</sup>	K <sub>obs</sub> (1/min)	Line Eqn
25	0.997	0.064	Y = 0.064x – 0.066
50	0.990	0.042	Y = 0.042x – 0.127
75	0.963	0.029	Y = 0.029x – 0.1216
100	0.977	0.023	Y = 0.0234x – 0.079

18, a straight line was obtained, where the slope of the line represented the rate constant (k). Also, the results revealed that the sonophotocatalyst degradation process of Acid Red 18 follows the pseudo-first-order kinetics. The concentration of Acid Red 18 oxidation was proportional to the surface of the ZnO catalyst covered by the dye, with the assumption that the dye is adsorbed to the catalyst with a higher intensity than by-products.

### 3.8. Mineralization

The decomposition of Acid Red 18 does not mean the complete destruction and mineralization of organic pollutants. Table 4 presents the TOC and COD removal efficiency of Acid Red 18 vs. reaction time in the hybrid AOP (ultraviolet/ZnO/ultrasonic) under optimized conditions.

Table 4 presents changes in TOC removal efficiency from the decomposition of Acid Red 18 vs. reaction time. The removal efficiency of TOC reached 60% during 45 min of reaction time. The rate of TOC removal as an indicator of the mineralization of organic compounds was slower than the COD and dye removal. This can be attributed to the presence of the by-products of dye degradation during the reaction. The free radicals such as OH<sup>•</sup> produced in the solution were not sufficient for degrading all of these compounds. In addition, the by-products formed were more resistant to UV irradiation than the original dye. After the dye was removed, the

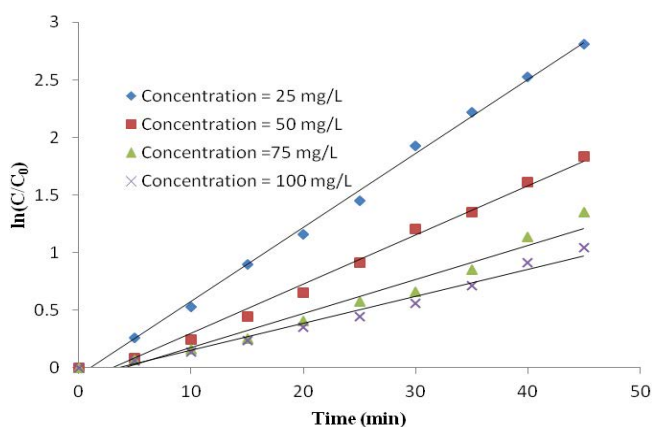


Fig. 13. Effect of various initial concentrations of Acid Red 18 on the reaction rate constant during the sonophotocatalyst process (concentration of ZnO catalyst stabilized on the glass plate was 1.66 g/L, pH = 10).

Table 4

Determination of TOC and COD removal rate by the sonophotocatalyst hybrid process at different times

Time (min)	COD removal efficiency (%)	TOC removal efficiency (%)
5	15	8
15	33	26
30	61	42
45	79	60

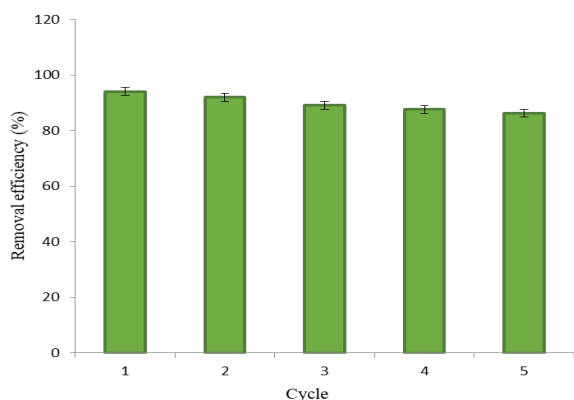


Fig. 14. Recycling and re-use of ZnO nanoparticles stabilized on a glass plate for the removal of Acid Red 18 by the sonophotocatalyst hybrid process.

hydroxyl radical was spent on the degradation of TOC compounds. It was also observed that the time for decolorization was shorter than that for TOC removal. Similar results were reported in the literature.

Table 4 also presents the changes in COD removal efficiency from the decomposition of Acid Red 18 vs. reaction time. The rate of COD removal was reduced by 79% in the 45-min period via the sonophotocatalyst hybrid process, clearly indicating the mineralization of Acid Red 18 by the sonophotocatalyst hybrid process.

### 3.9. Catalyst recycling and reuse

Reuse of the catalyst is an important parameter in processes such as photocatalysis and sonophotocatalysis, because reuse reduces the cost of treatment in a long period [23,44,45]. The effect of five times of recycling and reuse of ZnO nanoparticles stabilized on a glass plate in the presence of UV and US was evaluated, and the results are shown in Fig. 14. Based on the results, the rate of degradation at each step gradually decreased, such that at the (5th run) of reuse of nanoparticles, Acid Red 18 degradation rate reached 86.2%. Therefore, the results demonstrate that the stabilized ZnO catalyst can be recovered and reused in AOPs.

## 4. Conclusion

In this study, ZnO nanoparticles were thermally synthesized and stabilized on a glass plate, and their microstructures, morphologies, and chemical compositions were investigated. The high purity of the ZnO nanoparticles, their spherical structure, and uniform coating on the glass plate were confirmed, and the highest removal rate (94%) was obtained. The degradation reaction of Acid Red 18 by the sonophotocatalyst hybrid process followed the pseudo-first-order kinetics. Under optimal conditions, the removal efficiency of 79% and 60% for COD and TOC was obtained, respectively, during 45 min. Recycling and reuse of the stabilized catalyst on the glass plate were optimal, such that after the 5th run of the reuse of stabilized ZnO nanoparticles, Acid Red 18 removal rate was 86.2%, indicating an insignificant change relative to the 1st run of use. The advantages of this process are

high performance, low costs due to catalyst recycling, non-production of sludge, simple operation, and applicability on an industrial scale, and its disadvantage is a high catalyst consumption, because more catalysts (ZnO nanoparticles) were required to cover the entire the glass plate.

## Acknowledgments

This research was conducted in the Environmental Health Engineering Department of Sirjan Faculty of Medical Sciences and sponsored by the Vice-Chancellor for Research and Technology of Sirjan Faculty of Medical Sciences. The authors take this opportunity to express their gratitude for the support and assistance extended by the facilitators during the research period.

## References

- [1] N. Sobana, M. Swaminathan, The effect of operational parameters on the photocatalytic degradation of acid red 18 by ZnO, *Sep. Purif. Technol.*, 56 (2007) 101–107.
- [2] J.W. Lee, S.P. Choi, R. Thiruvengatchari, W.G. Shim, H. Moon, Evaluation of the performance of adsorption and coagulation processes for the maximum removal of reactive dyes, *Dyes Pigm.*, 69 (2006) 196–203.
- [3] S. Kaur, V. Singh, Visible light induced sonophotocatalytic degradation of Reactive Red dye 198 using dye sensitized TiO<sub>2</sub>, *Ultrason. Sonochem.*, 14 (2007) 531–537.
- [4] P.A. Carneiro, G.A. Umbuzeiro, D.P. Oliveira, M.V.B. Zanoni, Assessment of water contamination caused by a mutagenic textile effluent/dyehouse effluent bearing disperse dyes, *J. Hazard. Mater.*, 174 (2010) 694–699.
- [5] S.S. Martínez, E.V. Uribe, Enhanced sonochemical degradation of azure B dye by the electroFenton process, *Ultrason. Sonochem.*, 19 (2012) 174–178.
- [6] B. Chen, X. Wang, C. Wang, W. Jiang, S. Li, Degradation of azo dye direct sky blue 5B by sonication combined with zero-valent iron, *Ultrason. Sonochem.*, 18 (2011) 1091–1096.
- [7] S. Mozia, M. Tomaszewska, A.W. Morawski, Photocatalytic degradation of azo-dye Acid Red 18, *Desalination*, 185 (2005) 449–456.
- [8] S. Kavitha, P. Palanisamy, Photocatalytic and sonophotocatalytic degradation of reactive red 120 using dye sensitized TiO<sub>2</sub> under visible light, *Int. J. Civil Environ. Eng.*, 3 (2011) 1–6.
- [9] I.M. Khokhawala, P.R. Gogate, Degradation of phenol using a combination of ultrasonic and UV irradiations at pilot scale operation, *Ultrason. Sonochem.*, 17 (2010) 833–838.
- [10] C.G. Joseph, G.L. Puma, A. Bono, D. Krishnaiah, Sonophotocatalysis in advanced oxidation process: a short review, *Ultrason. Sonochem.*, 16 (2009) 583–589.
- [11] S. Dehghani, A.J. Jafari, M. Farzadkia, M. Gholami, Sulfonamide antibiotic reduction in aquatic environment by application of Fenton oxidation process, *Iranian J. Environ. Health Sci. Eng.*, 10 (2013) 29–34.
- [12] A. Nasiri, F. Tamaddon, M.H. Mosslemin, M.A. Gharaghani, A. Asadipour, Magnetic nano-biocomposite CuFe<sub>2</sub>O<sub>4</sub>@methylcellulose (MC) prepared as a new nano-photocatalyst for degradation of ciprofloxacin from aqueous solution, *Environ. Health Eng. Manage.*, 6 (2019) 41–51.
- [13] V. Revathi, K. Karthik, Microwave assisted CdO–ZnO–MgO nanocomposite and its photocatalytic and antibacterial studies, *J. Mater. Sci. Mater. Electron.*, 29 (2018) 18519–18530.
- [14] Y.G. Adewuyi, Sonochemistry in environmental remediation. 1. Combinative and hybrid sonophotochemical oxidation processes for the treatment of pollutants in water, *Environ. Sci. Technol.*, 39 (2005) 3409–3420.
- [15] J.T. Li, Y.L. Song, Degradation of AR 97 aqueous solution by combination of ultrasound and Fenton reagent, *Environ. Prog. Sustain.*, 29 (2010) 101–106.

- [16] M. Lee, J. Oh, Sonolysis of trichloroethylene and carbon tetrachloride in aqueous solution, *Ultrason. Sonochem.*, 17 (2010) 207–212.
- [17] J.-j. Lin, X.-s. Zhao, D. Liu, Z.-g. Yu, Y. Zhang, H. Xu, The decoloration and mineralization of azo dye CI Acid Red 14 by sonochemical process: rate improvement via Fenton's reactions, *J. Hazard. Mater.*, 157 (2008) 541–546.
- [18] A. Maleki, A. Mahvi, A. Mesdaghinia, K. Naddafi, Degradation and toxicity reduction of phenol by ultrasound waves, *Bull. Chem. Soc. Ethiopia*, 21 (2007) 33–38.
- [19] M.A. Matouq, Z.A. Al-Anber, T. Tagawa, S. Aljbour, M. Al-Shannag, Degradation of dissolved diazinon pesticide in water using the high frequency of ultrasound wave, *Ultrason. Sonochem.*, 15 (2008) 869–874.
- [20] J. Liang, S. Komarov, N. Hayashi, E. Kasai, Improvement in sonochemical degradation of 4-chlorophenol by combined use of Fenton-like reagents, *Ultrason. Sonochem.*, 14 (2007) 201–207.
- [21] N. Talebian, M.R. Nilforoushan, F.J. Mogaddas, Comparative study on the sonophotocatalytic degradation of hazardous waste, *Ceram. Int.*, 39 (2013) 4913–4921.
- [22] M. Malakootian, A. Nasiri, M. Amiri Gharaghani, Photocatalytic degradation of ciprofloxacin antibiotic by TiO<sub>2</sub> nanoparticles immobilized on a glass plate, *Chem. Eng. Commun.*, (2019) in Press.
- [23] G. Odling, Z.Y. Pong, G. Gilfillan, C.R. Pulham, N. Robertson, Bismuth titanate modified and immobilized TiO<sub>2</sub> photocatalysts for water purification: broad pollutant scope, ease of re-use and mechanistic studies, *Environ. Sci. Water Res. Technol.*, 4 (2018) 2170–2178.
- [24] R. Darvishi Cheshmeh Soltani, A. Rezaee, M. Safari, A. Khataee, B. Karimi, Photocatalytic degradation of formaldehyde in aqueous solution using ZnO nanoparticles immobilized on glass plates, *Desal. Wat. Treat.*, 53 (2015) 1613–1620.
- [25] R. Meena, H. Verma, H. Disha, Studies on photocatalytic degradation of azo dye Acid Red-18 (PONCEAU 4R) using Methylene Blue immobilized resin Dowex-11, *Int. J. Environ. Res.*, 2 (2013) 35–41.
- [26] M.A. Behnajady, N. Modirshahla, M. Mirzamohammady, B. Vahid, B. Behnajady, Increasing photoactivity of titanium dioxide immobilized on glass plate with optimization of heat attachment method parameters, *J. Hazard. Mater.*, 160 (2008) 508–513.
- [27] A. Khataee, M.-N. Pons, O. Zahraa, Photocatalytic degradation of three azo dyes using immobilized TiO<sub>2</sub> nanoparticles on glass plates activated by UV light irradiation: influence of dye molecular structure, *J. Hazard. Mater.*, 168 (2009) 451–457.
- [28] M. Malakootian, M.A. Gharaghani, A. Dehdarirad, M. Khatami, M. Ahmadian, M.R. Heidari, H. Mahdizadeh, ZnO nanoparticles immobilized on the surface of stones to study the removal efficiency of 4-nitroaniline by the hybrid advanced oxidation process (UV/ZnO/O<sub>2</sub>), *J. Mol. Struct.*, 1176 (2019) 766–776.
- [29] M.A. Gharaghania, M. Malakootiana, Photocatalytic degradation of the antibiotic ciprofloxacin by ZnO nanoparticles immobilized on a glass plate, *Desal. Wat. Treat.*, 89 (2017) 304–314.
- [30] X. Chen, Z. Wu, D. Liu, Z. Gao, Preparation of ZnO photocatalyst for the efficient and rapid photocatalytic degradation of azo dyes, *Nanoscale. Res. Lett.*, 12 (2017) 143.
- [31] V. Srivastava, D. Gusain, Y.C. Sharma, Synthesis, characterization and application of zinc oxide nanoparticles (n-ZnO), *Ceram. Int.*, 39 (2013) 9803–9808.
- [32] R. Suntuako, Effect of zinc oxide nanoparticles synthesized by a precipitation method on mechanical and morphological properties of the CR foam, *Bull. Mater. Sci.*, 38 (2015) 1033–1038.
- [33] N. Shimizu, C. Ogino, M.F. Dadjour, T. Murata, Sonocatalytic degradation of methylene blue with TiO<sub>2</sub> pellets in water, *Ultrason. Sonochem.*, 14 (2007) 184–190.
- [34] J. Wang, Z. Pan, Z. Zhang, X. Zhang, F. Wen, T. Ma, Y. Jiang, L. Wang, L. Xu, P. Kang, Sonocatalytic degradation of methyl parathion in the presence of nanometer and ordinary anatase titanium dioxide catalysts and comparison of their sonocatalytic abilities, *Ultrason. Sonochem.*, 13 (2006) 493–500.
- [35] A.M. Silva, E. Nouli, A.C. Carmo-Apolinário, N.P. Xekoukoulotakis, D. Mantzavinos, Sonophotocatalytic/H<sub>2</sub>O<sub>2</sub> degradation of phenolic compounds in agro-industrial effluents, *Catal. Today*, 124 (2007) 232–239.
- [36] K.P. Mishra, P.R. Gogate, Intensification of sonophotocatalytic degradation of p-nitrophenol at pilot scale capacity, *Ultrason. Sonochem.*, 18 (2011) 739–744.
- [37] J. Wang, Y. Jiang, Z. Zhang, X. Zhang, T. Ma, G. Zhang, G. Zhao, P. Zhang, Y. Li, Investigation on the sonocatalytic degradation of acid red B in the presence of nanometer TiO<sub>2</sub> catalysts and comparison of catalytic activities of anatase and rutile TiO<sub>2</sub> powders, *Ultrason. Sonochem.*, 14 (2007) 545–551.
- [38] N. Moradi, M.M. Amin, A. Fatehizadeh, Z. Ghasemi, Degradation of UV-filter Benzophenone-3 in aqueous solution using TiO<sub>2</sub> coated on quartz tubes, *J. Environ. Health Sci.*, 16 (2018) 213.
- [39] S. Norzaee, B. Djahed, R. Khaksefidi, F.K. Mostafapour, Photocatalytic degradation of aniline in water using CuO nanoparticles, *J. Water Supply Res. Technol.*, 66 (2017) 178–185.
- [40] B. Neppolian, H. Choi, S. Sakthivel, B. Arabindoo, V. Murugesan, Solar light induced and TiO<sub>2</sub> assisted degradation of textile dye reactive blue 4, *Chemosphere*, 46 (2002) 1173–1181.
- [41] M. Malakootian, A. Nasiri, H. Mahdizadeh, Metronidazole adsorption on CoFe<sub>2</sub>O<sub>4</sub>/Activated carbon@chitosan as a new magnetic biocomposite: modelling, analysis, and optimization by response surface methodology, *Desal. Wat. Treat.*, 164 (2019) 215–227.
- [42] M. Malakootian, H. Mahdizadeh, A. Dehdarirad, M. Amiri Gharaghani, Photocatalytic ozonation degradation of ciprofloxacin using ZnO nanoparticles immobilized on the surface of stones, *J. Dispers. Sci. Technol.*, 40 (2019) 846–854.
- [43] M. Malakootian, Z. Honarmandrad, Investigating the use of ozonation process with calcium peroxide for the removal of reactive blue 19 dye from textile wastewater, *Desal. Wat. Treat.*, 118 (2018) 336–341.
- [44] A. Nasiri, F. Tamaddon, M.H. Mosslemin, M.A. Gharaghani, A. Asadipour, New magnetic nanobiocomposite CoFe<sub>2</sub>O<sub>4</sub>@methylcellulose: facile synthesis, characterization, and photocatalytic degradation of metronidazole, *J. Mater. Sci. Mater. Elect.*, 30 (2019) 8595–8610.
- [45] M. Malakootian, A. Nasiri, A. Asadipour, E. Kargar, Facile and green synthesis of ZnFe<sub>2</sub>O<sub>4</sub>@CMC as a new magnetic nanophotocatalyst for ciprofloxacin degradation from aqueous media, *Proc. Saf. Environ. Protect.*, 129 (2019) 138–151.